Paper 1

Meland MY, Jansen E, Elderfield H (2005) Constraints on SST estimates for the northern North Atlantic/Nordic Seas during the LGM. Quaternary Science Reviews 24: 835-852

ELSEVIER

Quaternary Science Reviews 24 (2005) 835–852

QSR

Constraints on SST estimates for the northern North Atlantic/ Nordic Seas during the LGM

Marius Y. Meland[a,b,*], Eystein Jansen[a,b], Henry Elderfield[c]

[a]*Bjerknes Centre for Climate Research, University of Bergen, Allégaten 55, 5007 Bergen, Norway*
[b]*Department of Earth Sciences, University of Bergen, Allégaten 41, 5007 Bergen, Norway*
[c]*Department of Earth Sciences, University of Cambridge, Downing Street, Cambridge CB2 3EQ, UK*

Received 24 October 2003; accepted 7 May 2004

Abstract

A map of estimated calcification temperatures of the planktic foraminifer *Neogloboquadrina pachyderma* sinistral (T_{Nps}) for the Nordic Seas and the northern North Atlantic for the Last Glacial Maximum was produced from oxygen isotopes with support of Mg/Ca ratios. To arrive at the reconstruction, several constraints concerning the plausible salinity and $\delta^{18}O$-fields were employed. The reconstruction indicates inflow of temperate waters in a wedge along the eastern border of the Nordic Seas and at least seasonally ice-free waters. The reconstruction from oxygen isotopes shows similarities with Mg/Ca based paleotemperatures in the southern and southeastern sector, while unrealistically high Mg/Ca values in the central Nordic Seas prevent the application of the method in this area. The oxygen isotope based reconstruction shows some agreement with temperature reconstructions based on the modern analogue technique, but with somewhat lower temperatures and a stronger internal gradient inside the Nordic Seas. All told, our results suggest a much more ice-free and dynamic high latitude ocean than the CLIMAP reconstruction.

1. Introduction

The state of the sea surface in the North Atlantic and Nordic Seas provide important constraints on the climate in Europe and Eurasia, and strongly influence the strength of the meridional overturning circulation. The reliability of reconstructions for past climate states are crucial for developing a physical understanding of past climate changes, their dynamics, magnitude and underlying driving mechanisms. Reliable sea surface reconstructions are also critical as boundary conditions for atmospheric General Circulation Model (GCM) experiments of the Last Glacial Maximum (LGM) and as data for validation of experiments with fully coupled GCMs.

The problem of acquiring reliable SST reconstructions in the low temperature end is a long-standing issue. Due to the problem of low planktic foraminifer diversity in Arctic and Polar water masses, SST estimates based on planktic foraminiferal transfer functions are unreliable when summer temperatures are below 4–5 °C (e.g. Pflaumann et al., 1996, 2003). Other approaches also have their inherent problems: diatoms are often absent in LGM samples, the alkenone and dinocyst assemblage methods have difficulties in the low temperature end (Rosell-Melé and Comes, 1999; de Vernal et al., 2000), and the sensitivity of Mg/Ca ratios to temperature change is less at low temperatures than at higher (e.g. Elderfield and Ganssen, 2000; and see below).

Despite its wide usage, it has been clear for some time that the reconstruction of CLIMAP (1981) (Fig. 1a) based on the transfer function method of Imbrie and Kipp (1971) may be unreliable in the high latitude North Atlantic/Nordic Seas. In the CLIMAP reconstruction there is a permanent sea-ice cover over most of the area,

*Corresponding author. Bjerknes Centre for Climate Research, University of Bergen, Allégaten 55, 5007 Bergen, Norway. Tel.: +47-55-58-98-06; fax: +47-55-58-43-30.
E-mail address: marius.meland@bjerknes.uib.no (M.Y. Meland).

0277-3791/$ - see front matter © 2004 Elsevier Ltd. All rights reserved.
doi:10.1016/j.quascirev.2004.05.011

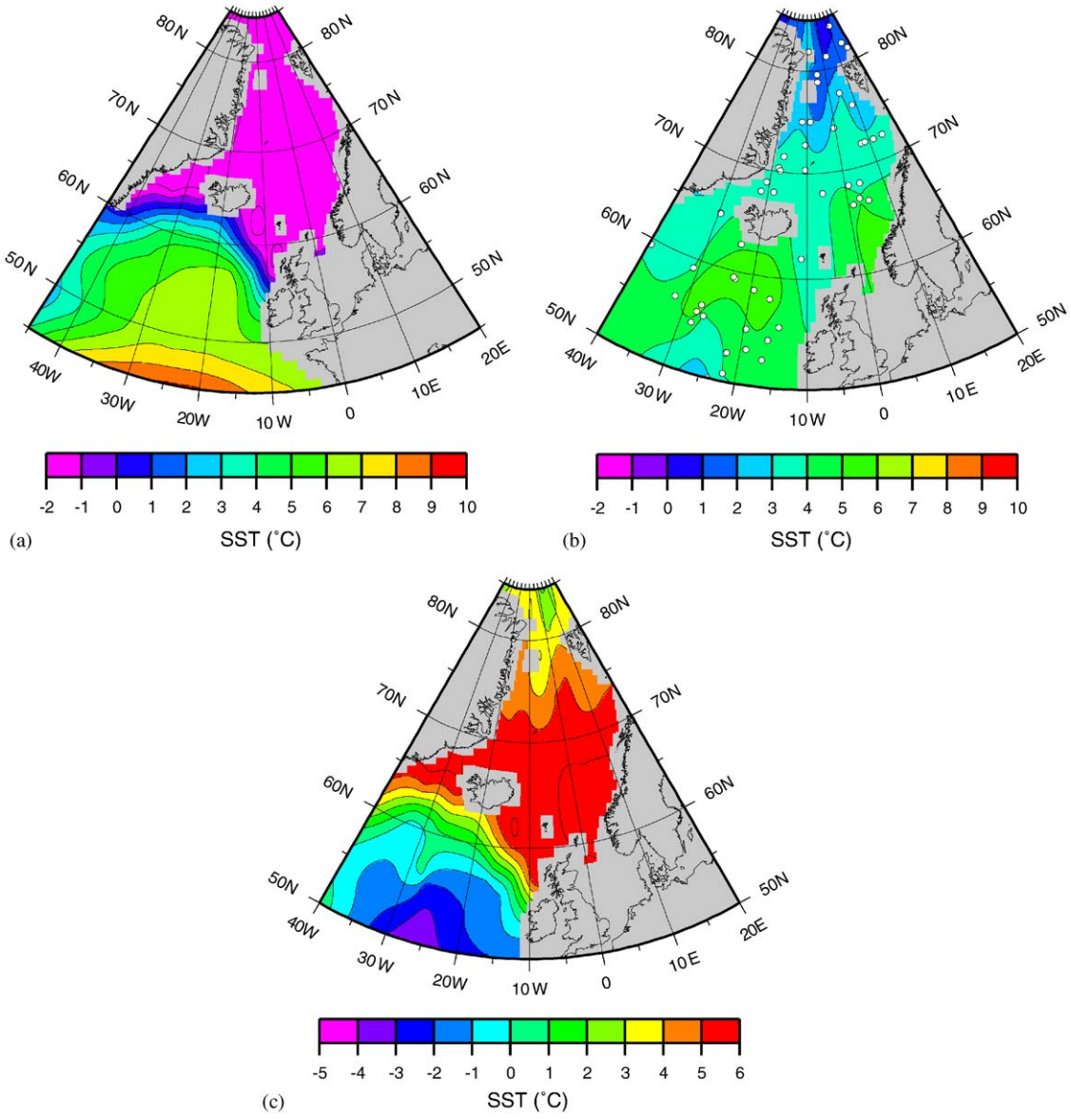

Fig. 1. (a) Summer (August) SST reconstruction for the LGM of CLIMAP (1981). CLIMAP placed the summer sea ice margin along the 0 °C isoline, with a perennial sea-ice cover inside this isoline. (b) Summer SST reconstruction for the LGM, based on gridding and contouring of the published SST data set of GLAMAP (Pflaumann et al., 2003). The SSTs were calculated from foraminiferal transfer functions using the SIMMAX-28 modern analogue technique. The white dots show the data locations. (c) Difference in SST between the GLAMAP and CLIMAP reconstructions, calculated as: $\Delta SST = SST_{GLAMAP} - SST_{CLIMAP}$. Grey coloured areas indicate land areas during the LGM (Peltier, 1994).

although newer evidence clearly point at least to seasonally open waters (e.g. Figs. 1b, 1c; Veum et al., 1992; Hebbeln et al., 1994; Wagner and Henrich, 1994; Sarnthein et al., 1995; Weinelt et al., 1996). The diversity problem of the transfer function approach, i.e. that there is only one dominant species, *Neogloboquadrina pachyderma* (sinistral coiled), in the Polar water, make these alternate reconstructions at least partially unreliable in the sense that they provide a more qualitative reconstruction rather than an accurate or realistic SST field.

The difference between a perennially frozen ocean and an open or seasonally open ocean has, however, wide climatic implications, for example in the possibility for the ocean to steer storm tracks and provide moisture supply to the high latitude ice sheets, to interact with marine based ice sheets and not least to constrain the location of deep water formation and the possible strength and northward extent of the meridional overturning circulation. Renewed attempts to better constrain the LGM state of the Nordic Seas and the northern North Atlantic should therefore be pursued.

Here we develop constraints on the plausible range of SST reconstructions for the LGM, primarily based on planktic foraminiferal oxygen isotopes. Although the oxygen isotopic composition of foraminiferal calcite depends on the oxygen isotopic composition of the ambient water (i.e. salinity), besides being a function of temperature, it is possible to evaluate the plausible salinity ranges constraining the data, and thus obtain estimates of SST from the oxygen isotopic composition by employing these constraints. We then compare these results with results using the Mg/Ca method and recent (post-CLIMAP) transfer function SST-estimates to identify the degree to which these different approaches provide a coherent picture.

2. Chronology

GLAMAP 2000 used two LGM time slices, comprising the intervals of 18.0–21.5 cal. ka (15–18 ^{14}C ka) and 19.0–22.0 cal. ka (16–19 ^{14}C ka) (Vogelsang et al., 2000). The first of these time slices is used in this work to temporally constrain the LGM, which in oxygen isotope records from the Nordic Seas is known to be a period of stability and minimum meltwater influx (Sarnthein et al., 1995). Since in some southern Atlantic records deglacial warming is already recorded in the younger part of the GLAMAP LGM time slice, the EPILOG working group (Mix et al., 2001) suggested a slightly different definition of the LGM: 19.0–23.0 cal. ka (16.0–19.5 ^{14}C ka). In northern Atlantic records, the early warming is not apparent in influencing oxygen isotope records (Sarnthein et al., 1995; Vogelsang et al., 2000; Pflaumann et al., 2003), which means that choice of time slice has limited importance, as long as the most important aspect is to cover a time slice of relatively stable climatic conditions. Since previous work on the LGM in the North Atlantic area mainly used the definition of 18.0–21.5 ka (e.g. Sarnthein et al., 1995, 2000, 2003; Weinelt et al., 1996; Nørgaard-Pedersen et al., 2003; Pflaumann et al., 2003), from which our data partly is drawn from, we find it most practical to use this definition of the LGM here.

The Mg/Ca data are from the time slice 19.0–21.5 ka, a period covered of both the GLAMAP and EPILOG time scales, but this slight difference has no influence on the results.

3. LGM data sets

3.1. Oxygen isotopes of N. pachyderma (sin.) ($\delta^{18}O_{Nps}$)

The LGM time slice is based on a total of 158 cores, covering the northern North Atlantic and the Nordic Seas (Fig. 2a). Table 1 shows the data sources. Fifty-three of these cores are dated by Accelerator Mass Spectrometry (AMS) ^{14}C within the range of the LGM

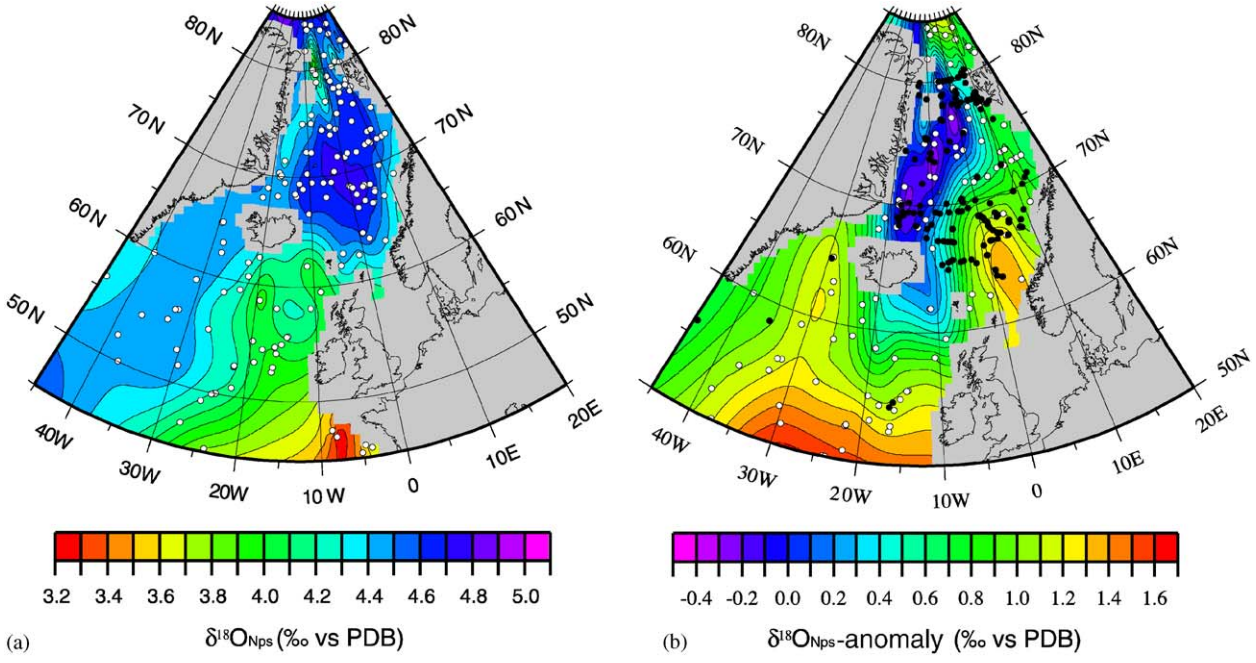

Fig. 2. (a) Oxygen isotope values ($\delta^{18}O_{Nps}$) for the LGM, based on the planktonic foraminifer *N. pachyderma* (sin.). The gridding, contouring and colouring are based on 158 cores, marked as white circles (Location in Table 1) (b) $\delta^{18}O_{Nps}$-anomaly between the LGM and modern values, calculated from the gridded plots as: plot($\delta^{18}O_{Nps(anomaly)}$) = plot($\delta^{18}O_{Nps(LGM)}$) − plot($\delta^{18}O_{Nps(modern)}$) − 1.1, where 1.1 is the ice volume effect. Black dots mark cores which contain $\delta^{18}O_{Nps(modern)}$ values, while white dots mark cores which contain $\delta^{18}O_{Nps(LGM)}$ values. The $\delta^{18}O_{Nps(modern)}$ values are from Simstich et al. (2003). Grey coloured areas indicate land areas during the LGM (Peltier, 1994).

Table 1
Cores used for studies of oxygen isotope ratios in the tests of *N. pachyderma* (sinistral).The isotopic temperatures (T_{Nps}) are determined by use of Eqs. (1)–(3) in text

Core no.	Longitude	Latitude	Water depth (m)	LGM level 18–21.5 ka depth (cm)	Number of averaged $\delta^{18}O_{Nps}$ measurements	Averaged $\delta^{18}O_{Nps}$	T_{Nps}	Data source for $\delta^{18}O_{Nps}$
BOFS 5 K	−21.87	50.68	3547	77–94[a]	9	4.17	5.1	Maslin (1992)
BOFS 8 K	−22.04	52.50	4045	78–110	13	4.21	4.3	Maslin (1992)
BOFS 14 K	−19.44	58.62	1756	34–44	5	3.94	5.3	Maslin (1992)
BOFS 16 K	−23.14	59.28	2502	42–48	2	4.26	3.7	Vogelsang (1990)
BOFS 17 K	−16.50	58.00	1150	68–95	13	4.17	4.9	Maslin (1992)
CH 67-19	−3.95	45.75	1982	380	1	3.57	7.4	Labeyrie and Duplessy (1985)
CH 69-12	−4.69	46.02	3642	Unknown	Unknown	3.65	6.9	Duplessy et al. (1991)
CH 69-32	−5.18	45.40	4777	Unknown	Unknown	3.56	7.5	Duplessy et al. (1991)
CH 72-101	−8.56	47.47	2428	280	1	3.51	7.7	Labeyrie and Duplessy (1985)
CH 72-104	−8.08	46.90	4590	380	1	3.25	8.9	Labeyrie and Duplessy (1985)
CH 73-108	−10.73	58.08	2032	Unknown	Unknown	4.18	4.5	Duplessy et al. (1991)
CH 73-110	−8.93	59.50	1365	102–110	Unknown	4.00	5.1	Weinelt (1993)
CH 73-136	−14.47	55.57	2201	120	1	4.18	4.7	Keigwin and Boyle (1989)
CH 73-139	−16.35	54.63	2209	160–190[a]	4	3.99	5.6	Bard et al. (1987)
CH 73-141	−16.52	52.86	3489	Unknown	Unknown	4.00	5.7	Duplessy et al. (1991)
CH 77-07	−10.52	66.60	1487	145–200	Unknown	4.62	1.0	Ruddiman and McIntyre (1981)
DSDP 609	−24.00	50.00	3884	88–101[a]	>5	4.25	4.6	Bond et al. (1993)
ENAM 93-21	−4.00	62.74	1020	220–250[a]	7	4.48	2.9	Rasmussen et al. (1996)
FRAM 1/4	−8.95	84.50	3820	15–23[a]	6	4.41	−1.9	Zahn et al. (1985)
FRAM 1/7	−6.96	83.88	2990	26–40	4	4.61	−1.8	Zahn et al. (1985)
HM 25-09	4.79	63.05	600	254–264	2	4.49	2.4	Jansen and Erlenkeuser (1985)
HM 31-33	4.78	63.63	1580	112	1	4.44	3.0	Jansen and Erlenkeuser (1985)
HM 31-36	0.53	64.25	2620	29–34	2	4.75	1.9	Jansen and Erlenkeuser (1985)
HM 52-43	0.73	64.25	2781	83–90[a]	3	4.51	2.7	Veum et al. (1992)
HM 57-07	−13.53	68.25	1668	34–42	Unknown	4.48	1.6	Sarnthein et al. (1995)
HM 71-12	−13.87	68.43	1547	44–48	3	4.69	1.6	Sarnthein et al. (1995)
HM 71-14	−18.08	69.98	1624	64	1	4.65	0.4	Sarnthein et al. (1995)
HM 71-19	−9.51	69.48	2210	42	1	4.81	0.9	Vogelsang (1990)
HM 80-30	1.60	71.78	2821	36–44	5	4.57	2.2	Sarnthein et al. (1995)
HM 80-42	−9.23	72.25	2416	54–64	6	4.44	0.3	Sarnthein et al. (1995)
HM 80-60	−11.86	68.90	1869	68–76	5	4.69	1.4	Sarnthein et al. (1995)
HM 94-13	−1.62	71.63	1946	44–52	5	4.66	1.6	Sarnthein et al. (1995)
HM 94-18	5.70	74.50	2469	25–35	2	4.58	1.9	Sarnthein et al. (1995)
HM 94-25	1.32	75.60	2469	38–47[a]	4	4.68	1.6	Sarnthein et al. (1995)
HM 94-34	−2.54	73.77	3004	50–53[a]	2	4.71	1.2	Sarnthein et al. (1995)
HM 100-7	−4.72	61.67	1125	63–100	38	4.39	3.4	Sarnthein et al. (1995)
K 11	1.60	71.78	2900	30–56	Unknown	4.66	1.9	Ruddiman and McIntyre (1981)
KN 708-1	−23.75	50.00	4053	100	1	4.11	5.2	Ruddiman and McIntyre (1981)
KN 708-6	−29.57	51.57	2469	60	1	4.46	3.0	Keigwin and Boyle (1989)
KN 714-15	−25.78	58.77	2598	415–419	1	4.23	3.7	Keigwin and Boyle (1989)
M 17045	−16.65	52.43	3663	80–110[a]	15	4.01	5.8	Winn et al. (1991)
M 17048	−18.16	54.30	1859	71–96	Unknown	4.02	5.3	Sarnthein et al. (1995)
M 17049	−26.73	55.28	3331	150–163[a]	14	4.29	2.9	Jung (1996)
M 17051	−31.98	56.17	2300	200–209[a]	3	4.34	2.7	Jung (1996)
M 17701	11.68	68.53	1421	92–141	Unknown	4.34	2.2	Sarnthein et al. (1995)
M 17719	12.57	72.15	1823	260–320	Unknown	4.46	2.5	Sarnthein et al. (1995)
M 17724	8.33	76.00	2354	47–58[a]	6	4.63	2.1	Weinelt (1993)
M 17725	4.58	77.47	2580	25–35[a]	4	4.41	1.7	Weinelt et al. (1996)
M 17728	3.95	76.52	2485	12–17	Unknown	4.69	1.0	Sarnthein et al. (1995)
M 17730	7.31	72.05	2769	132–147[a]	5	4.60	2.2	Weinelt (1993)
M 17732	4.23	71.62	3103	137–142	Unknown	4.75	1.7	Sarnthein et al. (1995)
M 23041	0.22	68.68	2258	30–36	Unknown	4.70	2.0	Sarnthein et al. (1995)
M 23043	−3.35	70.27	2133	30–38	Unknown	4.56	2.0	Sarnthein et al. (1995)
M 23055	4.10	68.42	2311	35–40	5	4.76	1.9	Vogelsang (1990)
M 23056	3.83	68.50	2665	27–35[a]	2	4.68	2.0	Weinelt et al. (1996)
M 23057	3.31	68.40	3157	24–29	Unknown	4.70	2.1	Sarnthein et al. (1995)
M 23059	−3.12	70.30	2283	29–32	4	4.72	1.4	Vogelsang (1990)
M 23062	0.16	68.73	2244	30–35	4	4.73	1.9	Vogelsang (1990)
M 23063	0.00	68.75	2299	31	1	4.76	1.8	Vogelsang (1990)

Table 1 (*continued*)

Core no.	Longitude	Latitude	Water depth (m)	LGM level 18–21.5 ka depth (cm)	Number of averaged $\delta^{18}O_{Nps}$ measurements	Averaged $\delta^{18}O_{Nps}$	T_{Nps}	Data source for $\delta^{18}O_{Nps}$
M 23064	0.33	68.67	2571	32–35	Unknown	4.66	2.2	Sarnthein et al. (1995)
M 23065	0.81	68.50	2804	29–34[a]	6	4.72	2.0	Vogelsang (1990)
M 23068	1.50	67.83	2230	61–75	2	4.74	2.0	Vogelsang (1990)
M 23071	2.93	67.08	1308	98–147[a]	5	4.73	2.7	Vogelsang (1990)
M 23074	4.92	66.67	1157	125–350[a]	19	4.62	2.3	Vogelsang (1990)
M 23254	9.63	73.12	2273	80–95	Unknown	4.70	1.7	Sarnthein et al. (1995)
M 23256	10.95	73.18	2061	70–90	Unknown	4.73	1.5	Sarnthein et al. (1995)
M 23258	13.98	75.00	1768	710–840	Unknown	4.52	2.1	Sarnthein et al. (1995)
M 23259	9.25	72.03	2518	140–170	7	4.68	1.8	Weinelt (1993)
M 23260	11.46	72.13	2089	110–140	5	4.71	1.6	Weinelt (1993)
M 23261	13.11	72.17	1628	192–260	10	4.60	1.9	Weinelt (1993)
M 23262	14.43	72.23	1130	200–320[a]	10	4.33	2.9	Weinelt (1993)
M 23269	0.68	71.45	2872	43–49	2	4.83	1.2	Weinelt (1993)
M 23294	−10.59	72.37	2224	110–123[a]	3	4.71	0.1	Weinelt (1993)
M 23323	5.93	67.77	1286	Unknown	Unknown	4.42	3.0	Sarnthein et al. (1995)
M 23351	−18.21	70.36	1672	55–78	6	4.40	−0.4	Voelker (1999)
M 23354	−10.63	70.33	1747	70–80[a]	2	4.50	1.2	Voelker (1999)
M 23415	−19.20	53.17	2472	135–164[a]	12	4.13	5.2	Jung (1996)
M 23419	−19.74	54.97	1491	40–42	1	3.96	5.5	Jung (1996)
M 23519	−29.60	64.80	1893	58–84	3	4.53	1.6	Hohnemann (1996)
MD 2010	4.56	66.68	1226	217–373[a]	47	4.61	2.3	Dokken and Jansen (1999)
MD 2011	7.64	66.97	1048	972–1361[a]	195	4.42	2.9	Dreger (1999)
MD 2012	11.43	72.15	2094	262–468[a]	37	4.58	2.0	Dreger (1999)
MD 2284	−0.98	62.37	1500	800–1050[a]	25	4.34	3.5	Jansen and Meland (2001)
MG 123	0.81	79.27	3050	58–72	2	4.65	0.9	Morris (1988)
NA 87-22	−14.57	55.50	2161	370–419[a]	20	4.06	4.8	Duplessy et al. (1992)
NO 77-14	−20.42	62.45	1531	Unknown	Unknown	4.65	2.5	Duplessy et al. (1991)
NO 79-06	−36.89	54.52	2734	290	1	4.45	1.8	Labeyrie and Duplessy (1985)
NO 79-25	−27.28	46.98	2826	Unknown	Unknown	4.10	6.3	Duplessy et al. (1991)
NP 90-12	9.42	78.41	628	220–275	7	4.65	1.1	Dokken (1995)
NP 90-36	9.94	77.62	1360	330–360	5	4.60	1.5	Dokken (1995)
NP 90-39	9.90	77.26	2119	127–155	8	4.48	2.0	Dokken (1995)
OD 41:4:1	11.24	84.03	3344	13–17[a]	3	4.76	−1.4	Nørgaard-Pedersen et al. (2003)
PS 1171	−18.07	68.20	935	22–50[a]	12	4.49	1.5	Lackschewitz et al. (1994)
PS 1230	−4.78	78.86	1235	20–28[a]	9	4.28	0.1	Nørgaard-Pedersen et al. (2003)
PS 1294	5.37	78.00	2668	35–55	5	4.75	0.3	Hebbeln and Wefer (1997)
PS 1295	2.43	78.00	3112	36–43	4	4.63	0.6	Jones and Keigwin (1989)
PS 1308	−4.83	80.02	1444	20–32	Unknown	3.95	−0.5	Nørgaard-Pedersen et al. (2003)
PS 1314	4.50	80.00	1382	21–28	Unknown	4.22	1.1	Nørgaard-Pedersen et al. (2003)
PS 1533	15.18	82.03	2030	60–85[a]	7	4.60	0.1	Köhler (1992)
PS 1535	1.85	78.75	2557	32–47[a]	8	4.60	1.5	Köhler (1992)
PS 1730	−17.7	70.12	1617	103–110[a]	1	4.29	−0.3	Stein et al. (1996)
PS 1894	−8.30	75.81	1975	36–125[a]	43	4.39	−0.4	Nørgaard-Pedersen et al. (2003)
PS 1919	−11.90	75.00	1876	13–33[a]	2	4.39	−0.7	Stein et al. (1996)
PS 1922	−8.77	75.00	3350	117–149[a]	2	4.40	−0.4	Stein et al. (1996)
PS 1927	−17.12	71.50	1734	65–95[a]	4	4.35	−0.6	Stein et al. (1996)
PS 1951	−20.82	68.84	1481	70–102[a]	4	4.48	1.4	Stein et al. (1996)
PS 2122	7.55	80.39	705	159–200	Unknown	4.20	1.4	Knies (1994)
PS 2123	9.86	80.17	571	187–228	Unknown	4.43	1.6	Knies (1994)
PS 2129	17.47	81.37	861	20–40[a]	Unknown	4.68	0.8	Knies (1999)
PS 2206	−2.51	84.28	2993	10–13	1	4.60	−1.8	Stein et al. (1994)
PS 2208	4.60	83.64	3681	15–25	Unknown	4.60	−1.1	Stein et al. (1994)
PS 2210	10.70	83.04	3702	12–14	1	4.65	−0.9	Stein et al. (1994)
PS 2212	15.85	82.07	2550	80–100	Unknown	4.26	0.0	Vogt (1997)
PS 2423	−5.45	80.04	829	20–100	Unknown	3.80	−0.6	Notholt (1998)
PS 2424	−5.74	80.04	445	390–433	Unknown	4.20	−0.6	Notholt (1998)
PS 2613	−0.48	74.18	3259	30–40[a]	3	4.71	1.2	Voelker (1999)
PS 2644	−21.77	67.87	778	111–129[a]	19	4.50	0.5	Voelker (1999)
PS 2837	2.38	81.23	1023	389–397[a]	9	4.72	0.0	Nørgaard-Pedersen et al. (2003)
PS 2876	−9.43	81.91	1976	9–62[a]	>20	4.55	−1.5	Nørgaard-Pedersen et al. (2003)

Table 1 (*continued*)

Core no.	Longitude	Latitude	Water depth (m)	LGM level 18–21.5 ka depth (cm)	Number of averaged $\delta^{18}O_{Nps}$ measurements	Averaged $\delta^{18}O_{Nps}$	T_{Nps}	Data source for $\delta^{18}O_{Nps}$
PS 2887	−4.61	79.60	1411	35–52[a]	18	3.33	−0.1	Nørgaard-Pedersen et al. (2003)
PS 16396	−11.25	61.87	1145	198–540[a]	38	4.08	4.5	Sarnthein et al. (1995)
PS 16397	−11.18	61.87	1145	4–98[a]	13	4.00	4.8	Sarnthein et al. (1995)
PS 21291	8.70	78.00	2400	85–105	Unknown	4.54	1.6	Weinelt (1993)
PS 21736	−5.17	74.33	3460	28	1	4.65	0.1	Jünger (1993)
PS 21842	−16.52	69.45	982	27–39[a]	2	4.44	0.6	Sarnthein et al. (1995)
PS 21900	−2.32	74.53	3538	25–33	2	4.45	0.7	Jünger (1993)
PS 21906	−2.15	76.93	2990	21–30[a]	9	4.25	0.6	Nørgaard-Pedersen et al. (2003)
PS 21910	1.32	75.62	2454	35–40	Unknown	4.50	1.6	Weinelt (1993)
PS 23199	5.24	68.38	1968	74–103	4	4.76	1.9	Vogelsang (1990)
PS 23205	5.76	67.62	1411	50–90	5	4.62	2.2	Vogelsang (1990)
PS 23243	−6.54	69.38	2715	55	1	4.71	1.2	Vogelsang (1990)
PS 23246	−12.86	69.40	1858	45	1	4.58	1.2	Vogelsang (1990)
RC 9-225	−15.40	54.89	2334	135	1	3.99	5.6	Keigwin and Boyle (1989)
SO 82-5	−30.9	59.18	1416	95–120[a]	6	4.43	1.9	van Kreveld et al. (2000)
SU 90-32	−22.42	61.78	2200	140–170	Unknown	3.98	4.8	Sarnthein et al. (1995)
SU 90-33	−22.08	60.57	2370	Unknown	Unknown	4.22	3.9	Cortijo et al. (1997)
SU 90-39	−21.93	52.57	2900	81–90	Unknown	4.25	4.5	Cortijo (1995)
SU 90-106	−39.45	59.98	1615	19–23	3	4.40	2.2	Weinelt et al. (1996)
SU 90-107	−28.08	63.08	1625	17–19	Unknown	4.17	3.5	Sarnthein et al. (1995)
V 23-23	−44.55	56.08	3292	115	1	4.34	2.0	Mix and Fairbanks (1985)
V 23-42	−27.92	62.18	1514	70	1	4.52	2.5	Keigwin and Boyle (1989)
V 23-81	−16.14	54.03	2393	236–304[a]	4	3.82	5.4	Jansen and Veum (1990)
V 23-82	−21.93	52.59	3974	110	1	4.34	4.2	Keigwin and Boyle (1989)
V 23-83	−24.26	49.87	3971	100	1	4.31	4.5	Keigwin and Boyle (1989)
V 27-17	−37.31	50.08	4054	35	1	4.42	3.1	Keigwin and Boyle (1989)
V 27-19	−38.79	52.10	3466	35	1	4.46	1.9	Keigwin and Boyle (1989)
V 27-60	8.58	72.17	2525	188–203	2	4.72	1.7	Labeyrie and Duplessy (1985)
V 27-86	1.12	66.60	2900	50–67	2	4.72	2.1	Labeyrie and Duplessy (1985)
V 27-114	−33.07	55.05	2532	291	1	4.42	2.2	Keigwin and Boyle (1989)
V 27-116	−30.33	52.83	3202	60	1	4.52	2.3	Keigwin and Boyle (1989)
V 28-14	−29.58	64.78	1855	149–170	3	4.60	1.2	Shackleton (1974)
V 28-38	−4.40	69.38	3411	184–192	Unknown	4.82	1.0	Keigwin and Boyle (1989)
V 28-56	−6.12	68.03	2941	60–80	4	4.67	1.5	Kellogg et al. (1978)
V 29-180	−23.87	45.30	3049	57	1	3.80	7.5	Keigwin and Boyle (1989)
V 29-183	−25.50	49.14	3629	38	1	4.10	5.4	Keigwin and Boyle (1989)
V 29-206	−29.28	64.90	1624	170	1	4.37	2.2	Keigwin and Boyle (1989)
V 30-108	−32.50	56.10	3171	85	1	4.52	2.0	Keigwin and Boyle (1989)
V 30-164	8.97	69.83	2901	Unknown	Unknown	4.83	1.3	Duplessy et al. (1991)

[a]The depths of the LGM levels are determined with use of AMS ^{14}C. Where no asterisk is shown, the LGM levels are determined by use of isotope stratigraphy.

level. In the other cores the LGM level is found based on the planktic oxygen isotope curves. Single $\delta^{18}O_{Nps}$-values from different low-resolution cores (see Table 1) are also included in the data set. In the publications from which the data was gathered, the authors simply defined the LGM as the event with the youngest distinct $\delta^{18}O_{Nps}$-maximum prior to Termination 1. We assume here that these values are inside the GLAMAP definition of the LGM, but admit that a higher robustness, resolution and more AMS ^{14}C dates are preferable. When integrating these data into the data set, we observe, however, that the spatial pattern is not changed, indicating that these data points are coherent with neighbouring data points that are better constrained by actual dates.

3.2. *Mg/Ca ratios of N. pachyderma (sin.)*

Foraminiferal Mg/Ca ratios are increasingly used as indicators of past ocean temperatures (e.g. Lea et al., 2000, 2002; Elderfield and Ganssen, 2000; Rosenthal et al., 2000). To add this information to the temperature information from the oxygen isotopes we applied Mg/Ca paleothermometry to a subset of samples from the LGM time slice and to a set of modern (core top) sediment samples.

The LGM part of the work is based on a total of 31 cores that provide a broad coverage of the North Atlantic north of 50°N, and the Nordic Seas. Table 2 shows the data. We measured the Mg/Ca ratios of the polar species *N. pachyderma* (sin.) in 1–6 samples from each core covering the LGM time slice, and note that some of the cores are not AMS ^{14}C dated (see Table 2). In these cases the LGM time slice definition was based on the planktic oxygen isotope records as described above. When choosing samples for Mg/Ca analyses, samples with planktic oxygen isotope values close to the average for the whole of the LGM level were given the highest priority. This was done to avoid potential internal fluctuations and obtain a best possible fit to oxygen isotope data.

Sediment surface samples from the Nordic Seas were also analysed for Mg/Ca content, with the purpose to investigate the correlation between the core top Mg/Ca ratios of *N. pachyderma* (sin.) and modern sea surface temperatures (SST). The data are shown in Table 3, and all these samples have Fe/Ca ratios below 0.1 mmol/mol, indicating that contamination should not influence the Mg/Ca ratios significantly (Barker et al., 2003). All samples are from box cores, covering the upper 0.5 cm of the sediment (Johannessen, 1992).

The samples were cleaned following the cleaning procedure of Barker et al. (2003), and were measured using the inductively coupled plasma-atomic emission spectroscopy (ICP-AES) method, with a relative precision of $<0.3\%$ (de Villiers et al., 2002). All cleaning and measurements were performed at the Department of Earth Sciences, University of Cambridge, UK.

4. Constraints on the temperatures derived from $\delta^{18}O$

The oxygen isotopic composition of foraminiferal calcite depends on both the temperature and the oxygen isotopic composition of the ambient seawater, $\delta^{18}O_w$. Since we here are primarily interested in the temperature, we need to address the factors that influence the $\delta^{18}O_w$, which are: the ice volume effect which results from the storage of water depleted in ^{18}O in ice sheets,

Table 2
Core data used for studies of Mg/Ca ratios in the tests of *N. pachyderma* (sinistral). The Mg/Ca ratios are analysed in this study

Core no.	Longitude	Latitude	Water depth (m)	LGM level 19–21.5 ka depth (cm)	Number of averaged trace element measurements	Average Mg/Ca (mmol/mol)	Reference LGM-level
BOFS 5 K	−21.87	50.68	3547	78–94[a]	4	0.87	Maslin (1992)
BOFS 7 K	−22.54	51.75	2429	38–40	2	0.91	Manighetti et al. (1995)
BOFS 8 K	−22.04	52.50	4045	85–110	2	0.81	Maslin (1992)
BOFS 10 K	−20.65	54.67	2761	108–114	4	0.93	Manighetti et al. (1995)
BOFS 14 K	−19.44	58.62	1756	38–44	3	0.92	Maslin (1992)
BOFS 17 K	−16.50	58.00	1150	74–95	4	1.16	Maslin (1992)
ENAM 94-09	−9.43	60.34	1286	543–583	3	0.89	Lassen et al. (2002)
HM 100-7	−4.72	61.67	1125	71–100	4	0.83	Sarnthein et al. (1995)
HM 52-43	0.73	64.25	2781	85–90[a]	2	0.81	Veum et al. (1992)
HM 71-12	−13.87	68.43	1547	44–48	3	0.96	Sarnthein et al. (1995)
HM 71-15	−17.43	70.00	1547	38–41[a]	4	0.71	Roe (1998)
HM 71-19	−9.51	69.48	2210	42	1	1.22	Vogelsang (1990)
HM 79-26	−5.93	66.90	3261	60	1	1.05	Sarnthein et al. (1995)
HM 80-30	1.60	71.78	2821	38–44	4	0.88	Sarnthein et al. (1995)
HM 80-42	−9.23	72.25	2416	57–64	4	0.90	Sarnthein et al. (1995)
HM 80-60	−11.86	68.90	1869	70–76	3	1.11	Sarnthein et al. (1995)
HM 94-13	−1.62	71.63	1946	46–52	4	0.98	Sarnthein et al. (1995)
HM 94-18	5.70	74.50	2469	28–35	2	0.96	Sarnthein et al. (1995)
HM 94-25	1.32	75.60	2469	38–47[a]	4	0.95	Sarnthein et al. (1995)
HM 94-34	−2.54	73.77	3004	50	1	0.79	Sarnthein et al. (1995)
M 23357	−5.53	70.96	1969	57	1	1.29	Goldschmidt (1994)
MD 2010	4.56	66.68	1226	261–373[a]	6	0.73	Dokken and Jansen (1999)
MD 2011	7.64	66.97	1048	1066–1361[a]	5	0.80	Dreger (1999)
MD 2284	−0.98	62.37	1500	870–1050	5	0.74	Jansen and Meland (2001)
MD 2289	4.21	64.66	1395	610–690	4	0.72	Berstad (pers. com.)
MD 2304	9.95	77.62	853	420–512[a]	5	0.74	Fevang (2001)
NEAP 8 K	−23.54	59.47	2419	179–192	4	0.94	Vogelsang et al. (2000)
PS 21842	−16.52	69.45	982	31–39[a]	5	0.85	Sarnthein et al. (1995)
SO 82-4	−30.48	59.10	1503	181–188[a]	1	0.89	Moros et al. (1997)
SU 90-32	−22.42	61.78	2200	140–170	1	0.80	Sarnthein et al. (1995)
V 23-81	−16.14	54.03	2393	260–304[a]	3	0.95	Jansen and Veum (1990)

[a]The depths of these LGM levels are determined with use of AMS ^{14}C.

Table 3
Core top data used for studies of Mg/Ca ratios of *N. pachyderma* (sin.). The Mg/Ca ratios are analysed in this study. All core tops are from box cores, upper 0.5 cm of the sediment (Johannessen, 1992)

Core no.	Longitude	Latitude	Water depth (m)	Observed Mg/Ca (mmol/mol)	$\delta^{18}O_{Nps}$ ratios	T JAS 50 m depth[a]	Calcification temperature[b]	"Calculated" Mg/Ca (mmol/mol)[c]	Mg/Ca deviation (mmol/mol)[d]
HM 16132	−0.72	64.57	2798	1.00	2.11	8.2	8.5	1.27	−0.28
HM 49-14	−3.23	65.42	2863	1.06	2.46	6.6	6.8	1.08	−0.02
HM 49-15	−0.36	66.34	3260	1.16	2.41	7.4	7.2	1.12	0.04
HM 52-34	−8.28	65.35	1101	1.14	3.00	5.9	5.1	0.91	0.23
HM 57-14	−6.21	67.00	3005	1.21	2.68	4.3	5.1	0.91	0.30
HM 57-20	1.67	62.65	750	1.13	2.40[e]	9.2	7.3	1.13	0.00
HM 94-12	−3.92	71.53	1816	0.99	3.25[e]	3.8	3.6	0.78	0.20
HM 94-16	5.61	73.38	2356	0.89	3.13[e]	2.8	4.3	0.84	0.05
HM 94-25	1.32	75.60	2469	1.12	3.68[e]	1.6	1.7	0.65	0.47
HM 94-42	−22.5	68.75	1339	0.98	3.10[e]	1.2	2.0	0.67	0.31

[a]Calculated from Levitus and Boyer (1994).
[b]Calcification temperatures are calculated from the oxygen isotope ratios given in table, and Eqs. (1) and (3) in text.
[c]"Calculated" Mg/Ca ratios are the ratios which should be expected from the calcification temperatures, using the equation of Nürnberg (1995) (Eq. (4) in text).
[d]Calculated in this manner: Mg/Ca deviation = observed Mg/Ca − "calculated" Mg/Ca.
[e]$\delta^{18}O_{Nps}$ measurements are not performed for these core tops. These values are interpolated $\delta^{18}O_{Nps}$ data calculated from nearby core tops with $\delta^{18}O_{Nps}$ measurements from Simstich et al. (2003).

and the salinity and the slope of the $\delta^{18}O_w$–salinity relationship.

4.1. Constraints on the ice volume effect

Before temperature calculations can be made, the effect that storage of isotopically depleted water in continental ice sheets has on $\delta^{18}O_w$ between the LGM and today must be assessed. Fairbanks (1989) proposed that ice volume indicated a change in $\delta^{18}O_w$ of 1.2–1.3‰ between LGM and today. Schrag et al. (1996), on the other hand, suggested an amplitude of 1.0‰, based on pore water measurements in deep sea sediments. For this work we have chosen an intermediate value of 1.1‰ for the ice volume effect at the LGM. The range of the different estimates of the ice volume effect indicated above, would impose an uncertainty on the temperature reconstructions of about ± 0.5–$1\,^{\circ}C$ on the absolute values, but do not influence the spatial patterns we reconstructed.

4.2. Oxygen isotope distribution of N. pachyderma (sin.) during the LGM

During the LGM, the northern North Atlantic and the Nordic Seas were characterized by a marked contrast in the foraminiferal isotopic composition between the areas south of the Iceland–Scotland Ridge and the Nordic Seas (Fig. 2a). In the eastern North Atlantic the $\delta^{18}O_{Nps}$-values were 3.8–4.4‰, while $\delta^{18}O_{Nps}$-values in the central Nordic Seas were quite homogenous with values about 4.6–4.8‰. In the western and eastern flanks of the Nordic Seas the $\delta^{18}O_{Nps}$-values were lower, with values averaging about 4.2–4.5‰.

By subtracting an ice volume effect of 1.1‰ from the raw data, the pattern in Fig. 2b is derived, showing $\delta^{18}O_{Nps}$-anomalies in the Nordic Seas. These anomalies suggest that the ice volume corrected $\delta^{18}O_{Nps}$-values in the Greenland and Iceland Seas for the LGM were not very different from today, indicating that similar surface environments as today prevailed in the LGM in the present cold water part of the Nordic Seas. The largest changes are evident south of the Iceland–Scotland Ridge and in the eastern Norwegian Sea, indicating that the meridional heat transport was much weaker during the LGM compared with today.

4.3. Constraints on the relationship between salinity (S) and $\delta^{18}O_w$ for the LGM

Constraining this relationship (or mixing line) for the Nordic Seas and the northern North Atlantic is not a straightforward work, since the water masses have different characteristics. $\delta^{18}O_w$ and salinity data from the database of Schmidt et al. (1999), show that the oxygen isotope values of the fresh water end member ($\delta^{18}O_0$) vary from −16‰ south of the Greenland–Scotland Ridge, −23‰ in the Norwegian Sea, −33‰ in Greenland–Iceland Seas and −35‰ in the Arctic Ocean. Simstich et al. (2003) have published relationships with $\delta^{18}O_0$ of −12‰ in the eastern and central Nordic Seas, and $\delta^{18}O_0$ of −17‰ in the East Greenland Current (EGC).

For the LGM the salinity/$\delta^{18}O$ relationship is not known. The Greenland deep ice cores show glacial oxygen isotope ratios down to less than −40‰ (Dansgaard and Oeschger, 1989), which are substantially below the modern values around −30‰, suggesting

a steeper mixing line than today. On the other hand, more intensive sea-ice formation during the LGM may produce sea-ice with an isotopic signature of, e.g. typically −2‰, the same as in the surrounding sea water, thus producing a fresh water source with isotopically high values that effectively lowers the salinity/$\delta^{18}O$ slope. It is therefore not obvious that the LGM slope was steeper than the modern. Based on an Earth system model of intermediate complexity, CLIMBER-2, Roche et al. (2004) found that no drastic changes occurred in the $\delta^{18}O_w$:S relationship. In the absence of conclusive evidence for a shift in this relationship, we suggest that the modern mixing line for both the North Atlantic and the Nordic Seas seems most appropriate. We therefore use the equation of GEOSECS (1987) obtained from $\delta^{18}O_w$ and salinity for water samples collected in the upper 250 m of the Atlantic Ocean during the GEOSECS expedition:

$$\delta^{18}O_w = -19.264 + 0.558 \times \text{salinity}. \quad (1)$$

4.4. Constraints on the LGM salinity

Since we have no direct method of assessing the salinity, we need to constrain the possible range of salinities from other criteria. In this case we need to consider:

- The homogenous $\delta^{18}O_{Nps}$-values in the Nordic Seas (Fig. 2a), which indicate that the salinity (and temperature) range within the Nordic Seas was quite low.
- Oxygen isotope change between modern data and the LGM (Fig. 2b), which can be used to assess the possible range of salinity changes in certain areas (see below).
- The general high latitude cooling of the LGM implies that inflow of saline waters from the North Atlantic into the Nordic Seas was reduced compared with today, due to the fact that warmer waters in general are more saline.
- Possible existence of deep convection, which requires salinity above certain thresholds.
- Higher glacial salinities in the Fram Strait, due to less melting of sea ice, reduced river runoff, and no inflow of low saline water through Bering Strait due to the low sea level.

From plotting the $\delta^{18}O_{Nps}$-anomalies between the recent data and the LGM (Fig. 2b), we find that the smallest anomaly between LGM and modern values exist in an elongated area in the Iceland Sea and the Greenland Sea, where open-ocean convection in Arctic water masses occurs today. This similarity indicates similar oceanographic conditions in this area during the LGM, with SSSs of 34.4–34.9‰ (the global salinity rise of +1‰ due to the ice volume effect is not added here and in the following discussion) and summer-SSTs of 0–6 °C, which is typical for Arctic water masses (Swift and Aagard, 1981). Considering that most of the Nordic Seas had similar isotope values, this is an indication for presence of Arctic water masses, with SSS- and SST-values as mentioned above.

In the northernmost cores in our compilation, in the Fram Strait region, the planktic isotope values indicate higher sea surface salinity during the LGM than today, since applying modern salinities for these locations to calculate SSTs from the oxygen isotope paleotemperature equation give LGM SST-values lower than −1.8 °C, which is below the freezing point of sea water. To correct this improbable result, the salinities of the LGM must be set to higher values than now in this area.

In the central and eastern parts of the North Atlantic we believe that salinities must have been lower than today as a result of the reduced northward oceanic heat flux and reduced advection of saline water from the tropics to higher latitudes.

Based on high epibenthic carbon isotope values in the Nordic Seas (Veum et al., 1992) and benthic oxygen isotope values (Dokken and Jansen, 1999), it appears likely that deep-sea ventilation and some element of open ocean convection took place in the Nordic seas in the LGM. Dokken and Jansen (1999) proposed that deep-water formation shifted between open ocean convection and brine-release due to sea-ice formation, and that shifts in the relative importance of the two deep-water formation types accompanied the millennial scale climate shifts of the last glacial. The brine mechanism can operate with lower preformed salinities than is required for open ocean convection. The benthic $\delta^{18}O$-change between LGM and Holocene in the Nordic Seas is 0.3‰ lower than the ice volume effect of 1.1‰ (Fairbanks, 1989; Schrag et al., 1996). This implies that the isotopic composition of the deep water to some extent was influenced by the brine mechanism. Yet the high epibenthic carbon isotope values (Veum et al., 1992), and the generally higher oxygen isotope values compared to many of the stadials of the last glacial would imply that at least some convection in open ocean areas occurred. Open-ocean convection will bring isotopically heavy water to the deep sea, while overturning by the brine-mechanism brings a light isotopic signal originating from densification of fresher waters by sea-ice formation to the deep sea. A mix of these two modes of deep-water formation may have produced an average LGM-Holocene change in benthic oxygen isotopes, which is 0.3‰ less than what would be expected from ice volume alone. Hence the average salinity of surface waters was probably 34.5–34.9‰, i.e. somewhat lower than today, but not by a large extent, as this may have hindered overturning

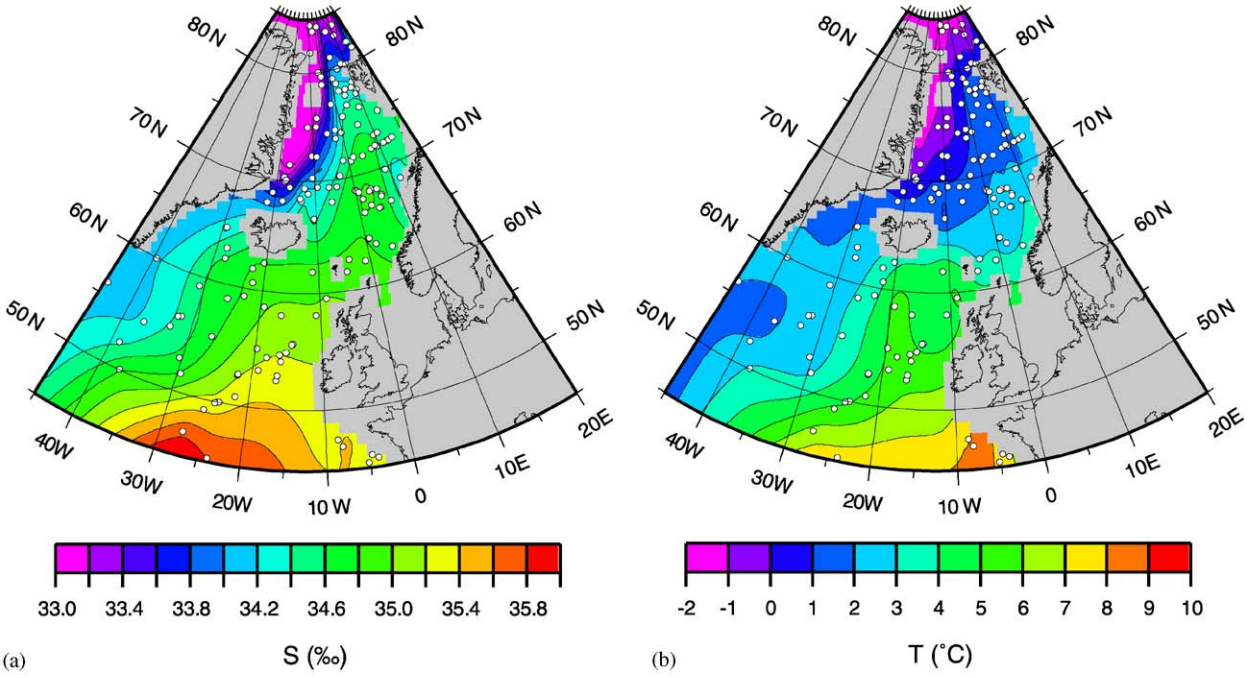

Fig. 3. (a) Suggested sea surface salinities for the LGM, based on the approach described in text (Sections 4.4.1 and 4.4.2). The higher global salinity (+1‰) during the LGM caused by the ice volume effect is not included. (b) Summer SST reconstruction for the LGM computed from the approach described in text (Section 4.5). The gridding, contouring and colouring were based on the estimated SST values (Table 1) calculated from Eq. (3) in text. Grey coloured areas indicate land areas during the LGM (Peltier, 1994).

and ventilation through some amount of open ocean convection.

Based on the discussion above, we have constrained the likely LGM salinity field follows (Fig. 3a):

- Lower salinities in the central and eastern Nordic Seas than today. They were, however, high enough to allow for some convection.
- The most likely open-ocean convection sites are where the highest $\delta^{18}O_{Nps}$-values are found (>4.7‰), assuming that convection occurred in the areas with highest $\delta^{18}O_{Nps}$-values, as it does today.
- Higher salinities in the Fram Strait and the border to the Arctic Ocean than today.
- Somewhat lower salinity in the North Atlantic relative to today, based on a lower northward advection of warm waters.
- Generally, lower salinity gradients between different areas compared with today, based on the homogenous LGM $\delta^{18}O_{Nps}$-field.

These constraints were used to calculate a possible salinity field in two steps:

4.4.1. 1st step: Salinities in the coldest water, where $T_{modern} \leqslant 2\,^{\circ}C$

We have here selected data from the core locations where the summer temperature (at 50 m depth, JAS) today is below 2 °C. It is highly unlikely that the temperatures during the LGM were significantly higher than today. There was probably partly ice-free water as far north as the Fram Strait (Hebbeln et al., 1994), thus the summer SST were above –1.8 °C. Therefore, we postulate that the SSTs have been between –1.8 and +2 °C for these cores and that as a first approximation the temperatures at their respective locations were similar to modern day temperatures.

We then used the modern day temperatures, the modern mixing line between salinity and $\delta^{18}O_w$ (Eq. (1)), and the paleotemperature equation of Shackleton (1974) to calculate salinities for these core locations. This results in a correlation of LGM and modern salinities of 0.62 in the northwestern area denoted in Fig. 3a. The best fit between modern and LGM salinities is expressed by the following equation:

$$S_{LGM} = 0.3192^{*}(S_{modern})^2 - 20.81^{*}S_{modern} + 371.8),\quad R^2 = 0.62. \tag{2}$$

4.4.2. 2nd step: Salinities for the area where $T_{modern} > 2\,^{\circ}C$

As a means of assessing the plausible range of salinities, we use Eq. (2) to calculate LGM salinities outside of the coldest end member area. The calculated salinities give similar salinity pattern as today, but with lower gradients between high and low salinity areas, in particular a reduced northward extent of saline surface waters compared with the modern values (Fig. 3a). We

stress that this is not based on a strictly objective criterion, yet the pattern agrees with the pattern that we expect to see considering the constraints discussed in the text above.

In favour of this attempt we can argue that the salinities in the coldest region cannot be much different, due to the fact that temperatures cannot be lower than freezing. There must also be a gradient between the low latitudes and the high latitude region as today, but with a smaller influx of saline waters in the Nordic seas areas due to the prevailing colder temperatures in the mid latitude region and the eastern boundary of the area which is consistent in all reconstructions of LGM temperatures. The calculated salinities give a similar salinity pattern as today, but with lower salinity gradients in the study area, as expected (Fig. 3a).

With the applied mixing line for oxygen isotopes vs. salinity an 0.48‰ error in salinity will result in a 1 °C change in the temperature estimate. With a steeper mixing line, e.g. closer to unity, an 0.25‰ salinity error will result in a 1 °C reconstructed temperature change. With the constraint that LGM salinities must be the same or less than modern (ice volume effect not included), and the observation that there must have been some deep convection, we contend that salinities cannot have been more than 0.3–0.5‰ lower than modern over the central and eastern parts of the Nordic Seas. Thus the salinity assumption used for our SST reconstruction produce an error of not more than 1 °C.

4.5. Temperature estimates

In the area where $T_{\text{modern}} \leqslant 2.0\,^{\circ}\text{C}$, we have defined that $T_{\text{LGM}} = T_{\text{modern}}$, based on arguments described in Section 4.4.1. Where $T_{\text{modern}} > 2.0\,^{\circ}\text{C}$, the salinities are defined as in Eq. (2) based on the arguments described in Section 4.4.2. $\delta^{18}O_w$ is then calculated using Eq. (1). The calcification temperatures of *N. pachyderma* (sin.) are then calculated using the paleotemperature equation of Shackleton (1974):

$$T = 16.9 - 4.38 * (\delta^{18}O_{\text{Nps}} - \delta^{18}O_w + 0.27) + 0.10 * (\delta^{18}O_{\text{Nps}} - \delta^{18}O_w + 0.27)^2. \quad (3)$$

The resulting temperatures are shown in Fig. 3b.

4.6. Discussion of oxygen isotope results

Assuming that the calcification of the foraminifers is a summer season phenomenon, in particular during the LGM, and that it takes place in the upper 100 m of the water column, at least for Arctic water masses (Johannessen, 1992; Simstich et al., 2003), the results in Fig. 3b can be viewed as an estimate of summer temperature of the surface mixed layer, possibly the lower part of it. Thus the peak summer temperatures of the surface may have been slightly higher than these estimates. The corridor of somewhat higher temperatures entering the Nordic seas in the SW in Fig. 3b is consistent with other evidence, such as the drift routes of icebergs inferred from sediment patterns of ice rafted constituents with known provenance in the North Sea (Hancock, 1984), and occurrence of significant amounts of subpolar planktic foraminifers in a band on the eastern side of the Nordic Seas as north as Fram Strait (Hebbeln et al., 1994). It is also consistent with the North Atlantic pattern in Fig. 3b, documenting that despite a more pronounced zonal temperature field than today, and a much more reduced northward heat flux in the ocean, there is an element of a meridional transport that is maintained. This meridionality is in conflict with the CLIMAP reconstruction, which had a perennial ice cover over the Nordic Seas at the LGM. The idea of some convection is also consistent with inferences from deep-water benthic foraminifer $\delta^{18}O$ of LGM conditions favourable for open ocean convection in the Nordic Seas (Dokken and Jansen, 1999). The low gradient towards the west is also consistent with the abundance patterns of biogenic carbonate (Hebbeln et al., 1998). The absolute temperatures south of the Greenland–Scotland Ridge are consistent with foraminiferal transfer function estimates (Pflaumann et al., 2003), while the temperatures within the Nordic Seas are slightly lower than those inferred from foraminiferal transfer functions, in particular in the western part of the ocean. This is most likely due to the lack of sensitivity of the transfer functions in cold waters.

The constraints on this reconstruction in terms of the possible range of salinity impose an error range of about $\pm 1\,^{\circ}\text{C}$ on the reconstruction. We conclude that this reconstruction, despite its shortcomings is a more likely LGM reconstruction than the CLIMAP, and probably also the GLAMAP reconstructions.

5. Constraints from Mg/Ca ratios

To further test the oxygen isotope based reconstruction, we also employed Mg/Ca paleothermometry on a subset of samples from the LGM as well as tests on the core top distribution of the Mg/Ca ratio. Applying the method in this type of environment is challenging, both due to the reduced slope of the Mg/Ca relationship vs. temperature in cold waters, thereby reducing its sensitivity and imposing larger error bars, but also due to the enhanced possibility of contamination from detrital minerals in the glacial marine sediments.

5.1. Contamination of clay and organic material

Even if the cleaning procedure of Barker et al. (2003) is used, there may still be significant amounts of clay

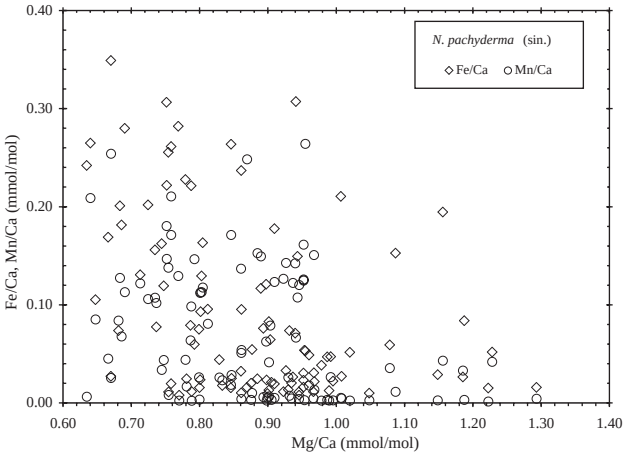

Fig. 4. Scatter of Fe/Ca and Mn/Ca plotted against Mg/Ca for all the LGM data, showing no covariance between these metals.

and/or organic material (hereafter called contaminant) in the analysed carbonate samples, which may influence the measured Mg/Ca values. Contamination will nearly always give higher Mg/Ca values, since the amount of Mg in silicate in nearly all cases is higher than the Mg content in carbonate. Indicators for contamination may be the content of Fe and Mn, documented in the Fe/Ca and Mn/Ca ratios of samples. These secondary metal ratios exhibit no positive correlation with Mg/Ca measured in *N. pachyderma* (sin.) for the LGM samples, and therefore suggest that contamination is not a significant control on Mg/Ca variability (Fig. 4). If it is assumed that the measured "contaminant" metals are representative of a silicate phase, then for a typical silicate Mg/Fe ratio of ~1 mol/mol, −30% of the measured Mg/Ca in *N. pachyderma* (sin.) could be attributed to contamination. However, it is probable that the Fe and Mn contaminant metals are in fact associated with a ferromanganese carbonate overgrowth (Boyle, 1983), particularly given the elevated Fe/Ca and Mn/Ca ratios observed.

5.2. Mg/Ca ratios in the core tops

While foraminiferal Mg/Ca ratios have shown great potential as indicators of past ocean temperatures in tropical and subtropical areas of the ocean (e.g. Lea et al., 2000, 2002; Elderfield and Ganssen, 2000; Rosenthal et al., 2000), the Mg/Ca ratios shown in Fig. 5a indicate a more complicated pattern. There seems to be very little temperature dependency across the basin, contrary to what would be expected. This lack of a temperature trend is due to the anomalously high values in the areas north to northeast of Iceland where the Mg/Ca ratios are much higher than expected if existing Mg/Ca based temperature equations are used (e.g. Elderfield and Ganssen, 2000; Nürnberg, 1995). The Mg/Ca ratios are not clearly correlated with calcification temperatures. We tested how well the observed core top Mg/Ca ratios fit with the paleotemperature equation of Nürnberg (1995) for the North Atlantic and the Nordic Seas:

$$\mathrm{Mg/Ca} = 0.549^{*}\mathrm{e}^{(0.099\times T)}. \quad (4)$$

We calculated from this equation the Mg/Ca ratios, which would correspond to the calcification temperatures deduced from core top oxygen isotopes (see Table 3), and found that 4 samples (marked with green circles in Fig. 5a) deviated with less than 0.06 mmol/mol from the expected Mg/Ca values. All these cores are located in Atlantic water masses. 1 sample (marked with a yellow circle in Fig. 5a) shows 0.28 mmol/mol lower than expected measured Mg/Ca ratios, while the samples to the west inside or close to Arctic water masses all have too high Mg/Ca values. The reason for these deviations from expected Mg/Ca values cannot be that the Nürnberg (1995) equation (Eq. (4)) does not work with the Arctic Water, since in this case we would expect that the deviations from sample to sample would be consistent in the whole region. Therefore other factors influence the Mg composition. At the moment, we suggest that Eq. (4) can be used for calculation of Mg/Ca based paleotemperatures in the eastern sector of the Nordic Seas, where 4 of the core tops deviate not more than 0.06 mmol/mol from the expected values based on the calibration curve of Nürnberg (1995). More data and analyses of various factors, such as salinity, dissolution, secondary encrustation, need to be explored.

We do not have core top measurements south of the Greenland–Scotland Ridge, but previous work suggest that the temperature dependency to Mg/Ca works better here (Nürnberg, 1995; Elderfield and Ganssen, 2000).

5.3. LGM results

The Mg/Ca ratios document a clear meridional trend in the eastern sector of the Norwegian Sea for the LGM, with somewhat lower ratios in the eastern Norwegian Sea (0.7–0.8 mmol/mol) than further south, in the North Atlantic west of Ireland (0.8–0.9 mmol/mol) (Fig. 5b). These Mg/Ca ratios were transferred to temperatures using Eq. (4) in the area south of the Greenland–Scotland Ridge and the Norwegian Sea.

5.3.1. Temperature estimates

The temperatures were calculated using Eq. (4), and are shown in Fig. 5c. Note that the Mg/Ca based temperatures are only calculated in the eastern Nordic Seas and south of the Greenland–Scotland Ridge, based on arguments mentioned in Section 5.2.

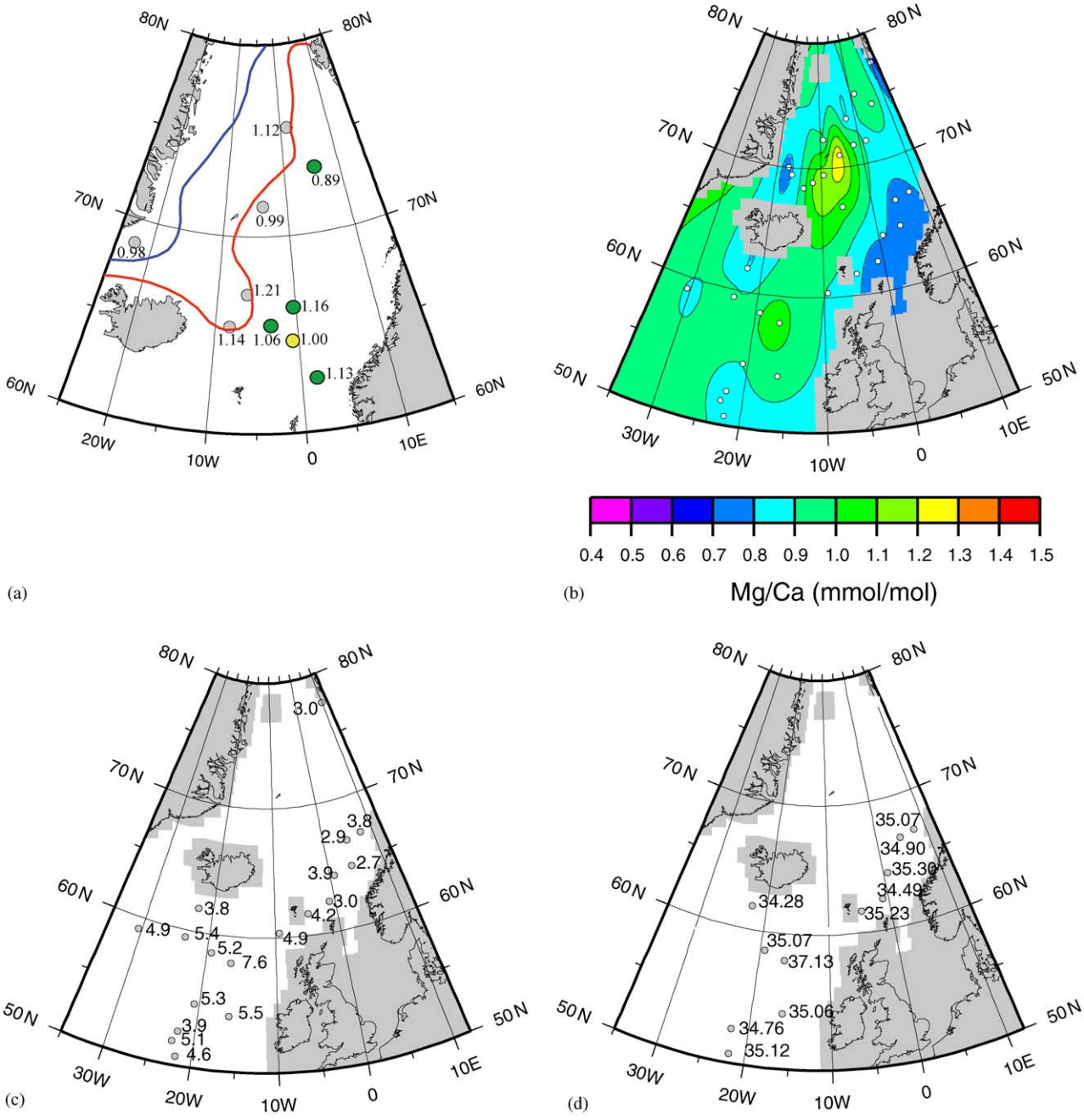

Fig. 5. (a) Mg/Ca ratios (mmol/mol) of core tops, measured on *N. pachyderma* (sin.). The green coloured circles are samples with measured Mg/Ca ratios deviating less than 0.06 mmol/mol from "expected" Mg/Ca ratios, calculated from Eq. (4) in text. The yellow coloured sample has a measured Mg/Ca ratio of 0.28 mmol/mol below the "expected" Mg/Ca ratios. The grey coloured samples show "too high" Mg/Ca ratios. See Table 3 for details. The red line marks the Arctic Front, separating Atlantic and Arctic water masses. The blue line marks the Polar Front, separating Arctic and Polar water masses. (b) Mg/Ca distribution for the LGM, based on averaged Mg/Ca ratios in Table 2 of *N. pachyderma* (sin.). The white dots show the locations of the cores. (c) Mg/Ca calcification temperatures of *N. pachyderma* (sin.), calculated using the Mg/Ca temperature equation of Eq. (4) in text. (d) Calcification salinities of *N. pachyderma* (sin.), calculated using the Mg/Ca temperatures in Fig. 5c and oxygen isotope ratios from Table 1. Not all points from Fig. 5c are shown on the map, since oxygen isotope data are not available for the LGM in some of the cores. The higher global salinity (+1‰) during the LGM is not included. See the text for details on salinity calculation. Grey coloured areas indicate land areas during the LGM (Peltier, 1994).

5.3.2. $\delta^{18}O_w$ and salinity estimates

Values of $\delta^{18}O_w$ and salinities are calculated for the cores in Fig. 5c where we have suggested that Eq. (4) can be used for calculation of Mg/Ca based temperatures. The $\delta^{18}O_w$ can easily be computed by a rearrangement of Eq. (3):

$$\delta^{18}O_w = \delta^{18}O_{Nps} + 0.27 - 21.9 + \sqrt{(310.61 + 10T_{Nps})}. \quad (5)$$

By assuming that the mixing line from GEOSECS (1987) (Eq. (1)) can be used, as argued above, we calculate salinities by rearrangement of Eq. (1):

$$S = [(\delta^{18}O_w + 34.52) \times 1.792] - 1. \quad (6)$$

Note that the global salinity rise of +1‰ due to the ice volume effect is subtracted on the end of this equation for comparison to the modern salinities. The resulting salinities are shown in Fig. 5d.

5.4. Discussion of Mg/Ca results

South of the Greenland–Scotland Ridge and in the eastern parts of the Nordic Seas the temperatures and salinities deviate somewhat from the estimates obtained from oxygen isotopes above, i.e. on average higher temperature and salinity. Yet, the meridional trend in the Eastern sector of the study area is similar to the oxygen isotope temperature trend (Figs. 3b, 5b–d). The Mg/Ca results for the LGM are consistent with a warmer and sea-ice free sector in the Eastern Nordic Seas, as compared with the CLIMAP reconstruction. The main problem with the Mg/Ca results is the higher Mg/Ca ratios to the west (not shown in Fig. 5c). Existing temperature equations (e.g. Eq. (4)) give temperatures about 5–10 °C, which are much higher than the summer SSTs today in this area (0–5 °C). It is clear that there must be an artefact on the ratios in the areas north of Iceland. We note that the same deviation from a temperature relationship is found in this area in the core top data (Fig. 5a). This may point to a specific problem with the method in this sub-area. Since all the Fe/Ca ratios of these samples are less than 0.1 mmol/mol, we find it difficult to ascribe the high Mg/Ca ratios to contamination. A possibility is that the high Mg/Ca ratios in the Greenland and Iceland Seas could be due to high salinity, because of salt rejection via sea-ice formation and brine. This process requires, however, intensive sea-ice formation to increase the salinity in significant amounts, and it is questionable whether there was enough sea-ice formation in the central ocean, since sea-ice formation is largely a shelf process. Another possibility is that sea-ice cover, of reasons not explored, may give high Mg/Ca ratios both for the core tops and the LGM. The area where the green and yellow core tops are marked (Fig. 5a), covers Atlantic water masses, while the area with grey core tops covers an area inside or close to Arctic water masses. The positions where the grey core tops are marked, may in several winters be sea-ice covered. Nürnberg (1995) found that core tops in areas partly covered by sea-ice showed anomalously high Mg/Ca ratios. The same may be true for the LGM time slice. The anomalously high Mg/Ca ratios for the LGM (Fig. 5b) may also reflect water masses, at least partly, covered by sea-ice. It may also be that physiological processes, food supply or gametogenic calcite play a more important role than temperature in this cold area, where the exponential character of the Mg/Ca temperature curves make the curves flatter in most published temperature equations. Further investigations in this region need to be performed to identify the possible causes for the anomalously high Mg/Ca values. We just note that the values northeast of Iceland are unreasonable in terms of a temperature reconstruction, i.e. both the modern and LGM data from the sub-area are too high.

6. Discussion

We have developed constraints on the range of possible salinity and $\delta^{18}O_w$ fields in the Nordic Seas and the North Atlantic. Given these constraints we obtain an oxygen isotope based reconstruction of summer temperatures of the upper 100 m of the water column that gives a reasonable fit to other observations of the paleoceanography of the region during the LGM (Fig. 3b). It indicates a reduced, but significant meridional advection in the east, i.e. similar to the modern pattern, but with much lower temperatures, and a low gradient between this area and the western area, which was colder. Oxygen isotope derived SSTs in the North Atlantic are consistent with newer transfer function estimates for this region (Pflaumann et al., 2003), while the oxygen isotope based reconstruction for the Nordic Seas is different from the transfer function estimates. The newer transfer function based reconstructions have no discernable east–west gradients, something which appears unlikely based on physical reasoning, since the pattern of inflowing waters in the east, which is seen both as a northward trending tongue of warmer temperatures south of the Iceland–Scotland Ridge and as a wedge of somewhat smaller reconstructed temperatures in the eastern Nordic Seas, would imply that there was a compensating southward flow of colder, Polar waters off east Greenland. Thus the reconstruction of Fig. 3b appears more likely. The mean temperature in the Nordic Seas is also lower in the oxygen isotope based reconstruction than in the transfer function based estimates. We ascribe both these differences to the lack of resolution for transfer functions at the cold end member, and contend that the oxygen isotope based reconstruction is more realistic. The CLIMAP reconstruction is in conflict with evidence from various sources that there must have been seasonally open waters in the Nordic Seas during the LGM (e.g. Fig. 1b; Veum et al., 1992; Hebbeln et al., 1994; Wagner and Henrich, 1994; Sarnthein et al., 1995; Weinelt et al., 1996), thus the oxygen isotope based reconstruction is much more in line with this evidence than the CLIMAP reconstruction, which had the whole Nordic Seas covered by a perennial sea-ice cover.

In agreement with the oxygen isotope based temperatures, the Mg/Ca based temperatures also indicate meridional advection in the east (Fig. 5c). Even if we have observed that the core tops in the eastern Nordic Seas deviate not much from the temperature calibration line of Nürnberg (1995), we suggest that more core top and downcore studies are required to develop a more consistent Mg/Ca temperature equation for the studied area, before the method can be used with sufficient reliability both in the eastern Nordic Seas and the northern North Atlantic. For the central and western Nordic Seas it is obvious that other factors than temperature influence the Mg/Ca ratios. It should also be mentioned that other methods have problems in this partly sea-ice covered area, like the alkenone method (Rosell-Melé and Comes, 1999), the dinocyst assemblage method (de Vernal et al., 2000) and partly the planktic foraminifer assemblage method (Pflaumann et al., 1996, 2003, Fig. 1b). Common for these methods and the Mg/Ca method is that they all suggest unreasonably high temperatures. Also factors like salinity, pH, physiological processes and gametogenic calcite may be important by influencing the Mg/Ca ratios, not only for the western and central Nordic Seas, but also for the eastern Nordic Seas and for some areas laying south of the Greenland–Scotland Ridge. Further studies are needed to elucidate the causes of these high Mg/Ca ratios.

We expect that replacing the commonly used CLIMAP data set for this region with the oxygen isotope based reconstruction (Fig. 3b) as ocean boundary conditions for climate models will change a number of aspects of the modelled dynamics of the LGM climate, such as storm tracks, degree of meridionality/zonality and existence of the well known modes of modern climate variability, e.g. the NAO/AO. The seasonally ice-free waters apparent in our reconstruction may act as a moisture source, consistent with the current understanding of the rapid growth of the Fennoscandian and Barents Ice Sheets, during the LGM (Boulton, 1979; Elverhøi et al., 1995; Mangerud et al., 2002). The growth clearly requires a strong source of winter precipitation, and a degree of meridional circulation. A zonal circulation, which is the result when using the CLIMAP reconstruction as boundary conditions, would probably provide too little winter precipitation to feed rapid growth of ice sheets in the northern portion of the Nordic Seas.

7. Conclusions

(1) The LGM temperatures, based on oxygen isotopes in the planktic foraminifer species *N. pachyderma* (sin.), imply that central and eastern parts of the Nordic Seas were ice-free, at least during the summer.
(2) The LGM temperatures, based on Mg/Ca ratios in *N. pachyderma* (sin.), show some meridionality south of the Greenland–Scotland Ridge and in the eastern parts of the Nordic Seas. More core top and downcore studies are needed before a more consistent Mg/Ca temperature equation for the studied area can be used with sufficient reliability. We thus suggest that the oxygen isotope based reconstruction of Fig. 3b is a better method to constrain LGM temperatures here.
(3) The temperature reconstruction based on oxygen isotopes is probably the most realistic approach for qualitative reconstructions of sea surface conditions in the Nordic Seas during the LGM. The results in this reconstruction appear consistent with dynamics required for the rapid growth of the Fennoscandian and Barents Ice Sheets during the LGM.

Acknowledgements

We thank Mervyn Greaves for patient training on the Mg/Ca cleaning method and for help with the Mg/Ca analyses, at the University of Cambridge. Stephen Barker is thanked for helpful advice on cleaning methods. Rune Søraas and Odd Hansen are thanked for keeping the stable isotope mass spectrometer in good shape. This manuscript was greatly improved by formal reviews from two anonymous reviewers, and by comments and suggestions from Carin Andersson Dahl, Ulysses Ninnemann and Trond Dokken. This project is financed by The Norwegian Academy of Science and Statoil under the VISTA program, the CESOP-project funded by the European Commission (EVR1-2001-40018), and the Bjerknes Centre.

References

Bard, E., Arnold, M., Maurice, P., Duprat, J., Moyes, J., Duplessy, J.-C., 1987. Retreat velocity of the North Atlantic polar front during the last deglaciation determined by ^{14}C accelerator mass spectrometry. Nature 328, 791–794.

Barker, S., Greaves, M., Elderfield, H., 2003. A study of cleaning procedures used for foraminiferal Mg/Ca paleothermometry. Geochemistry, Geophysics, Geosystems 4 (9), 8407.

Bond, G., Broecker, W.S., Johnsen, S., McManus, J., Labeyrie, L., Jouzel, J., Bonani, G., 1993. Correlations between climate records from North Atlantic sediments and Greenland ice. Nature 365, 143–147.

Boulton, G.S., 1979. Glacial history of the Spitsbergen archipelago and the problem of a Barents Shelf ice sheet. Boreas 8, 31–57.

Boyle, E.A., 1983. Manganese carbonate overgrowths on foraminifera tests. Geochimica et Cosmochimica Acta 47, 1815–1819.

CLIMAP, 1981. Seasonal reconstruction of the Earth's surface at the Last Glacial Maximum. Map Chart Series MC-36.

Cortijo, E., 1995. La variabilité climatique rapide dans l'Atlantique Nord depuis 128 000 ans: relations entre les calottes de glace et l'ocean de surface. Ph.D. Thesis, University of Paris, France, 235pp.

Cortijo, E., Labeyrie, L., Vidal, L., Vautravers, M., Chapman, M.R., Duplessy, J.-C., Elliot, M., Arnold, M., Turon, J.-L., Auffret, G., 1997. Changes in sea surface hydrology associated with Heinrich event 4 in the North Atlantic Ocean between 40° and 60°N. Earth and Planetary Science Letters 146, 29–45.

Dansgaard, W., Oeschger, H., 1989. Past environmental long-term records from the Arctic. In: Oeschger, H., Langway, Jr., C.C. (Eds.), The Environmental Record in Glaciers and Ice Sheets. Wiley, New York, pp. 287–318.

de Vernal, A., Hillaire-Marcel, C., Turon, J.-L., Matthiessen, J., 2000. Reconstruction of sea-surface temperature, salinity, and sea-ice cover in the northern North Atlantic during the last glacial maximum based on dinocyst assemblages. Canadian Journal of Earth Sciences 37, 725–750.

de Villiers, S., Greaves, M., Elderfield, H., 2002. An intensity ratio calibration method for the accurate determination of Mg/Ca and Sr/Ca of marine carbonates by ICP-AES. Geochemistry, Geophysics, Geosystems 3 2001GC000169.

Dokken, T., 1995. Last interglacial/glacial cycle on the Svalbard/Barents Sea margin. Ph.D.Thesis, University of Tromsø, Norway, 175pp.

Dokken, T., Jansen, E., 1999. Rapid changes in the mechanism of ocean convection during the last glacial period. Nature 401, 458–461.

Dreger, D., 1999. Decadal-to-centennial-scale sediment records of ice advance on the Barents shelf and meltwater discharge into the north-eastern Norwegian Sea over the last 40 kyr. Ph.D. Thesis, University of Kiel, Germany, 79pp.

Duplessy, J.-C., Labeyrie, L., Juillet-Leclerc, A., Maitre, F., Duprat, J., Sarnthein, M., 1991. Surface salinity reconstruction of the North Atlantic Ocean during the Last Glacial Maximum. Oceanologica Acta 14, 311–324.

Duplessy, J.-C., Labeyrie, L., Arnold, M., Paterne, M., Duprat, J., van Weering, T.C.E., 1992. Changes in surface salinity of the North Atlantic Ocean during the last deglaciation. Nature 358, 485–488.

Elderfield, H., Ganssen, G.M., 2000. Past temperature and $\delta^{18}O$ of surface ocean waters inferred from foraminiferal Mg/Ca ratios. Nature 405, 442–445.

Elverhøi, A., Andersen, E.S., Dokken, T., Hebbeln, D., Spielhagen, R.F., Svendsen, J.I., Sørflaten, M., Rørnes, A., Hald, M., Forsberg, C.F., 1995. The growth and decay of Late Weichselian ice sheet in Western Svalbard and adjacent areas based on provenance studies of marine sediments. Quaternary Research 44, 303–316.

Fairbanks, R.G., 1989. A 17,000-year glacio-eustatic sea level record: influence of glacial melting rates on the Younger Dryas event and deep-ocean circulation. Nature 342, 637–642.

Fevang, A., 2001. Klimaendringer i de nordiske hav i siste glasiale maksimum og Terminasjon 1. Unpublished Cand. Scient. Thesis in Marine Geology, University of Bergen, Norway, 106pp.

GEOSECS Atlantic, Pacific and Indian Ocean Expeditions, 1987. Shorebased data and graphics. In: GEOSECS Executive Committee, Ostlund, H.G., Craig, H., Broecker, S.W.S., Spencer, D. (Eds.), National Science Foundation 7.

Goldschmidt, P.M., 1994. The ice-rafting history in the Norwegian-Greenland Sea for the last two glacial/interglacial cycles. Berichte—Reports, 313, University of Kiel, Germany, 103pp.

Hancock, J.M., 1984. Cretaceous. In: Glennie, K.W. (Ed.), Introduction to the Petroleum Geology of the North Sea. Blackwell, Cambridge, pp. 133–150.

Hebbeln, D., Wefer, G., 1997. Late Quaternary Paleoceanography in the Fram Strait. Paleoceanography 12, 65–78.

Hebbeln, D., Dokken, T., Andersen, E.S., Hald, M., Elverhøi, A., 1994. Moisture supply for northern ice-sheet growth during the Last Glacial Maximum. Nature 370, 357–360.

Hebbeln, D., Henrich, R., Baumann, K.-H., 1998. Paleoceanography of the last glacial/interglacial cycle in the polar North Atlantic. Quaternary Science Reviews 17, 125–153.

Hohnemann, C., 1996. Zur Paläoceanographie der südlichen Dänemarkstraße. Unpublished Dipl. Arb. Thesis, University of Kiel, Germany.

Imbrie, J., Kipp, N.G., 1971. A new micropaleontological method for quantitative micropaleontology: application to a late Pleistocene Caribbean core. In: Turekian, K. (Ed.), Late Cenozoic Glacial Ages. Yale University Press, New Haven, pp. 71–81.

Jansen, E., Erlenkeuser, H., 1985. Ocean circulation in the Norwegian Sea during the last deglaciation: isotopic evidence. Palaeogeography, Palaeoclimatology, Palaeoecology 49, 189–206.

Jansen, E., Meland, M., 2001. Stratigraphy of IMAGES cores in the Faeroese-Shetland area. Technical Report 01-01, Bjerknes Centre for Climate Research, Bergen, Norway.

Jansen, E., Veum, T., 1990. Evidence for two-step deglaciation and its impact on North Atlantic deep-water circulation. Nature 343, 612–616.

Johannessen, T., 1992. Stable isotopes as climatic indicators in ocean and lake sediments. Dr. Scient Thesis, University of Bergen, Norway.

Jones, G.A., Keigwin, L., 1989. Evidence from Fram Strait (78°N) for early deglaciation. Nature 336, 56–59.

Jung, S.J.A., 1996. Wassermassenaustausch zwischen NE-Atlantik und Nordmeer während der letzten 300 000/80 000 Jahre im Abbild stabiler O- und C-isotope. Berichte aus dem Sonderforschungsbereich, 313, University of Kiel, 61, 104pp.

Jünger, B., 1993. Tiefenwassererneuerung in der Grønlandsee während der letzten 340 000 Jahre. Ph.D. Thesis, University of Kiel, Germany.

Keigwin, L., Boyle, E.A., 1989. Late Quaternary paleochemistry of high-latitude surface waters. Palaeogeography, Palaeoclimatology, Palaeoecology 73, 85–106.

Kellogg, T.B., Duplessy, J.-C., Shackleton, N.J., 1978. Planktonic foraminiferal and oxygen isotope stratigraphy and paleoclimatology of Norwegian deep-sea cores. Boreas 7, 61–73.

Knies, J., 1994. Spätquartäre Sedimentation am Kontinentalhang nordwestlich Spitzbergens, Der letzte Glazial/Interglazial-Zyklus. Thesis, Justus-Liebig-University, Giessen, Germany, 95pp.

Knies, J., 1999. Spätquartäre Paläoumweltbedingungen am nördlichen Kontinentalrand der Barents- und Kara-See: Eine Multi-Parameter-Analyse. Berichte Polarforschung, 304. Alfred Wegener Institute, Bremerhaven, Germany, 159pp.

Köhler, S.E.I., 1992. Spätquartäre paläo-ozeanographische Entwicklung des Nordpolarmeeres und Europäischen Nordmeeres anhand von Sauerstoff- und Kohlenstoffisotopenverhältnissen der planktischen Foraminifere *Neogloboquadrina pachyderma* (sin.). Geomar Research Centre for Marine Geosciences, Kiel, Germany, 104pp.

Labeyrie, L., Duplessy, J.-C., 1985. Changes in the oceanic $^{13}C/^{12}C$ ratio during the last 140,000 years: high-latitude surface water records. Palaeogeography, Palaeoclimatology, Palaeoecology 50, 217–240.

Lackschewitz, K.L., Dehn, J., Wallrabe-Adams, H.J., 1994. Volcaniclastic sediments from mid-oceanic Kolbinsey Ridge, north of Iceland: Evidence for submarine volcanic fragmentation processes. Geology 22, 975–978.

Lassen, S., Kuijpers, A., Kunzendorf, H., Lindgren, H., Heinemeier, J., Jansen, E., Knudsen, K.L., 2002. Intermediate water signal leads surface water response during Northeast Atlantic deglaciation. Global and Planetary Change 32, 111–125.

Lea, D.W., Pak, D.K., Spero, H.J., 2000. Climate impact of late quaternary equatorial Pacific sea surface temperature variations. Science 289, 1719–1724.

Lea, D.W., Martin, P.A., Pak, D.K., Spero, H.J., 2002. Reconstructing a 350 ky history of sea level using planktonic Mg/Ca and oxygen isotope records from a Cocos Ridge core. Quaternary Science Reviews 21, 283–293.

Levitus, S., Boyer, T.P., 1994. World Ocean Atlas 1994, vol. 4, Temperature, NOAA Atlas NESDIS 4. US Department of Commerce, Washington, DC, 117pp.

Mangerud, J., Astakhov, V., Svendsen, J.I., 2002. The extent of the Barents-Kara ice sheet during the Last Glacial Maximum. Quaternary Science Reviews 21, 111–119.

Manighetti, B., McCave, I.N., Maslin, M., Shackleton, N.J., 1995. Chronology for climate change: Developing age models for the Biogeochemical Ocean Flux Study cores. Paleoceanography 10, 513–525.

Maslin, M., 1992. A study of the paleoceanography of the N.E. Atlantic in the late Pleistocene. Ph.D. Thesis, University of Cambridge, England.

Mix, A.C., Fairbanks, R.G., 1985. North Atlantic surface-ocean control of Pleistocene deepocean circulation. Earth and Planetary Science Letters 73, 231–243.

Mix, A.C., Bard, E., Schneider, R., 2001. Environmental processes of the ice age: land, oceans, glaciers (EPILOG). Quaternary Science Reviews 20, 627–657.

Moros, M., Endler, R., Lackschewitz, K.L., Wallrabe-Adams, H.J., Mienert, J., Lemke, W., 1997. Physical properties of Reykjanes Ridge sediments and their linkage to high-resolution Greenland Ice Sheet Project 2 ice core data. Paleoceanography 12, 687–695.

Morris, T.H., 1988. Stable isotope stratigraphy of the Arctic Ocean: Fram Strait to Central Arctic. Palaeogeography, Palaeoclimatology, Palaeoecology 64, 201–219.

Notholt, H., 1998. The implication of the "North East Water"—Polynya on the sedimentation by NE-Greenland and late Quaternary paleo-oceanic investigations. Alfred Wegener Institute for Polar and Marine Research, Bremerhaven, Germany, 182pp.

Nürnberg, D., 1995. Magnesium in tests of *Neogloboquadrina pachyderma* sinistral from high northern and southern latitudes. Journal of Foraminiferal Research 25, 350–368.

Nørgaard-Pedersen, N., Spielhagen, R.F., Erlenkeuser, H., Grootes, P.M., Heinemeier, J., Knies, J., 2003. Arctic Ocean during the Last Glacial Maximum: Atlantic and polar domains of surface water mass distribution and ice cover. Paleoceanography 18, 1063.

Peltier, W.R., 1994. Ice Age paleotopography. Science 265, 195–201.

Pflaumann, U., Duprat, J., Pujol, C., Labeyrie, L., 1996. SIMMAX, a Transfer technique to deduce Atlantic Sea Surface Temperatures from planktonic foraminifera—the EPOCH approach. Paleoceanography 11, 15–35.

Pflaumann, U., Sarnthein, M., Chapman, M.R., d'Abreu, L., Funnell, B., Huels, M., Kiefer, T., Maslin, M., Schulz, H., Swallow, J., van Kreveld, S., Vautravers, M., Vogelsang, E., Weinelt, M., 2003. Glacial North Atlantic: sea-surface conditions reconstructed by GLAMAP 2000. Paleoceanography 18, 1065.

Rasmussen, T.L., Thomsen, E., van Weering, T.C.E., Labeyrie, L., 1996. Rapid changes in surface and deep water conditions at the Faeroe Margin during the last 58,000 years. Paleoceanography 11 (6), 757–771.

Roche, D., Paillard, D., Ganopolski, A., Hoffmann, G., 2004. Oceanic oxygen-18 at the present day and LGM: equilibrium simulations with a coupled climate model of intermediate complexity. Earth and Planetary Science Letters 218, 317–330.

Roe, A.B., 1998. Hurtige klimavariasjoner i havområdet øst for Scoresbysund, Grønland—isotoptrinn 3 og 2. Unpublished Cand. Scient. Thesis, University of Bergen, Norway, 93pp.

Rosell-Melé, A., Comes, P., 1999. Evidence for a warm Last Glacial Maximum in the Nordic seas or an example of shortcomings in U^{K}_{37}, and U^{K}_{37} to estimate low sea surface temperature. Paleoceanography 14, 770–776.

Rosenthal, Y., Lohmann, G.P., Lohmann, K.C., Sherrell, R.M., 2000. Incorporation and preservation of Mg in *Globigerinoides sacculifer*: Implications for reconstructing the temperature and the $^{18}O/^{16}O$ of seawater. Paleoceanography 15, 135–145.

Ruddiman, W.F., McIntyre, A., 1981. The North Atlantic during the last deglaciation. Palaeogeography, Palaeoclimatology, Palaeoecology 35, 145–214.

Sarnthein, M., Jansen, E., Weinelt, M., Arnold, M., Duplessy, J.-C., Erlenkeuser, H., Flatøy, A., Johannessen, G., Johannessen, T., Jung, S.J.A., Koc, N., Labeyrie, L., Maslin, M., Pflaumann, U., Schulz, H., 1995. Variations in Atlantic surface ocean paleoceanography, 50°–80°N: A time-slice record of the last 30,000 years. Paleoceanography 10, 1063–1094.

Sarnthein, M., Stattegger, K., Dreger, D., Erlenkeuser, H., Grootes, P.M., Haupt, B.J., Jung, S.J.A., Kiefer, T., Kuhnt, W., Pflaumann, U., Schäfer-Neth, C., Schulz, H., Schulz, M., Seidov, D., Simstich, J., van Kreveld, S., Vogelsang, E., Völker, A., Weinelt, M., 2000. Fundamental modes and abrupt changes in North Atlantic circulation and climate over the last 60 ky—concepts, reconstruction and numerical modelling. In: Schäfer, P., Ritzrau, W., Schlüter, M., Thiede, J. (Eds.), The Northern North Atlantic: A Changing Environment. Springer, Berlin, pp. 365–410.

Sarnthein, M., Pflaumann, U., Weinelt, M., 2003. Past extent of sea ice in the northern North Atlantic inferred from foraminiferal paleotemperature estimates. Paleoceanography 18, 1047.

Schmidt, G.A., Bigg, G.R., Rohling, E.J., 1999. Global Seawater Oxygen-18 Database. Web page: www.giss.nasa.gov/data/o18data.

Schrag, D.P., Hampt, G., Murray, D.W., 1996. Pore fluid constraints on the temperature and oxygen isotopic composition of the glacial ocean. Science 272, 637–642.

Shackleton, N.J., 1974. Attainment of isotopic equilibrium between ocean water and the benthonic foraminifera genus *Uvigerina*: isotopic changes in the ocean during the Last Glacial. Colloques Internationaux du CNRS 219, 203–209.

Simstich, J., Sarnthein, M., Erlenkeuser, H., 2003. Paired $\delta^{18}O$ signals of *Neogloboquadrina pachyderma* (s) and *Turborotalita quinqueloba* show thermal stratification structure in Nordic Seas. Marine Micropaleontology 48, 107–125.

Stein, R., Schubert, C., Vogt, C., Fütterer, D., 1994. Stable isotope stratigraphy, sedimentation rates and paleosalinity in the latest Pleistocene to Holocene Central Arctic Ocean. Marine Geology 119, 333–355.

Stein, R., Nam, S., Grobe, H., Hubberten, H., 1996. Late Quaternary glacial history and short-term ice rafted debris fluctuations along the East Greenland continental margin. In: Andrews, J.T., Austin, W.E.N., Bergsten, H., Jennings, A.E. (Eds.), Late Quaternary Paleoceanography of the North Atlantic Margins. Geological Society Special Publication, The Geological Society, Oxford, UK, pp. 135–152.

Swift, J.H., Aagard, K., 1981. Seasonal transitions and water mass formation in the Iceland and Greenland Seas. Deep-Sea Research I 28, 1107–1129.

van Kreveld, S., Sarnthein, M., Erlenkeuser, H., Grootes, P.M., Jung, S.J.A., Nadeau, M.J., Pflaumann, U., Voelker, A.H., 2000. Potential links between surging ice sheets, circulation changes, and the Dansgaard–Oeschger cycles in the Irminger Sea. Paleoceanography 15, 425–442.

Veum, T., Arnold, M., Beyer, I., Duplessy, J.-C., 1992. Water mass exchange between the North Atlantic and the Norwegian Sea during the last 28,000 years. Nature 356, 783–785.

Voelker, A.H., 1999. Zur Deutung der Dansgaard–Oeschger Ereignisse in ultrahochauflösenden Sedimentprofilen aus dem Europäischen Nordmeer. Ph.D. Thesis, University of Kiel, Germany, 180pp.

Vogelsang, E., 1990. Paläo-Ozeanographie des Europäischen Nordmeeres an Hand stabiler Kohlenstoff- und Sauerstoffisotope. Ph.D. Thesis, University of Kiel, Germany.

Vogelsang, E., Sarnthein, M., Pflaumann, U., 2000. $\delta^{18}O$ Stratigraphy, Chronology, and Sea Surface Temperatures of Atlantic Sediment Records (GLAMAP-2000 Kiel). Berichte—Reports, 13, University of Kiel, Germany.

Vogt, C., 1997. Zur Paläozeanographie und Paläoklima im spätquartären Arktischen Ozean: Zusammensetzung und Flux terrigener und biogener Sedimentkomponenten auf dem Morris Jesup Rise und dem Yermak Plateau. Berichte Polarforschung, 251. Alfred Wegener Institute, Bremerhaven, Germany, 309pp.

Wagner, T., Henrich, R., 1994. Organo- and lithofacies of TOC-lean glacial/interglacial deposits in the Norwegian-Greenland Sea: sedimentary and diagenetic responses to paleoceanographic and paleoclimatic changes. Marine Geology 120, 335–364.

Weinelt, M., 1993. Veränderungen der Oberflächenzirkulation im Europäischen Nordmeer während der letzten 60,000 Jahre – Hinweise aus stabilen Isotopen. Ph.D. Thesis, University of Kiel, Germany, 106pp.

Weinelt, M., Sarnthein, M., Pflaumann, U., Schulz, H., Jung, S.J.A., Erlenkeuser, H., 1996. Ice-free Nordic Seas during the Last Glacial Maximum? Potential sites of deepwater formation. Paleoclimates 1, 283–309.

Winn, K., Sarnthein, M., Erlenkeuser, H., 1991. $\delta^{18}O$ stratigraphy and chronology of Kiel sediment cores from the East Atlantic. Berichte—Reports 45, Department of Geology and Paleontology, University of Kiel, Germany, 99p.

Zahn, R., Markussen, B., Thiede, J., 1985. Stable isotope data and depositional environments in the late Quaternary. Nature 314, 433–435.